Leadership in Sustainable Infrastructure

Leadership en Infrastructures Durables

Vancouver, Canada
May 31 – June 3, 2017/ *Mai 31 – Juin 3, 2017*

AN OPTIMAL NUMERICAL SCHEME FOR MULTI-SPAN COMPOSITE LAMINATED FRP DECK BRIDGES

Naderian, HR.[1, 5], Cheung, M. S.[2], Dragomirescu, E.[3], Mohammadian, M.[4]
[1, 3, 4] University of Ottawa, Canada
[2] Western China Earthquake and Hazards Mitigation Research Centre, Sichuan University, China
[5] hnade057@uottawa.ca

Abstract: This research suggests a very efficient numerical technique, originated from spline finite strip method, for simulating fiber reinforced polymer (FRP) deck bridges. An Integrated Finite Strip Method (IFSM) is employed in order to evaluate the bending and vibration performance of continuous multi-span composite laminated FRP bridge systems. The anisotropy nature of the FRP laminated deck is considered into the analysis by developing so-called laminate spline strip in the environment of integrated finite strip solution. So-called column strips model the piers, while the structural interactions between the FRP deck and piers are handled into the analysis by introducing transition section elements. The accuracy and efficiency of the IFSM in modelling as well as bending, and free vibration analysis of a multi-span slab-girder FRP bridge is investigated. The finite strip results will be validated against the finite element analysis. Using the proposed integrated finite strip approach, the time required for analysis dramatically reduces without affecting the degree of accuracy. This results in developing an optimal numerical scheme for composite FRP bridges. The developed IFSM solution provides the opportunity for analysis and design FRP deck bridge structures in a very efficient way where the coupling effects of the FRP laminated deck and the structural interactions of bridge components are fully handled.

1. INTRODUCTION

The finite strip method (FSM) is an attractive numerical solution for bridge structures. High accuracy and efficiency due to its semi-analytical nature as well as rapid convergence owing to the small bandwidth elastic matrices, along with the simplicity of the input data and simulation have made FSM outstanding among conventional numerical techniques of bridge analysis. In spite of merits of FSM, it is mostly applicable for simple shapes of structural elements like plates and shells and folded-plate structures (Cheung et al. 1996). When it comes to a more complicated system like a continuous multi-span bridge where there are a number of structural elements attached together in different orientations, the FSM is no longer a powerful tool for 3D simulation of the structure. Therefore, the FSM was limited to model the bridge deck only while other structural components including piers were modeled as special boundary conditions of the deck. When external forces are applied to the bridge, the internal forces are transmitted between structural elements. Therefore, handling the structural interactions of all segments of the bridge system is a necessary step in accurate analysis of bridges. For all these reasons, the application of FSM in bridge analysis had almost reached the technical limit for more than a decade. Recently, Moe M. S. Cheung and his colleagues (Naderian et al. 2015) created an innovative integrated framework that is capable of 3D modelling of an entire bridge system in the environment of spline finite strip method where the effects of structural interactions between different segments of the bridge can also be considered.
Nowadays, the use of advanced composite FRP materials in multi-span bridges is encouraged by the bridge engineers. Research shows the stiffness of advanced composite materials including FRP is

coupled to the geometry of the structure (Reddy 2004). The latter indicates the importance of the accurate simulation of the composite structure geometry although it is a very expensive computational process. In contrast with traditional steel and concrete materials which are typically modelled as isotropic materials, FRP composites are highly anisotropic depending on the type of fibers, matrix, and the orientation of each lamina. Taking into account the above features, the structural performance of FRP laminated deck bridges is totally different from the conventional bridges due to the, lighter weight and more flexible structural system. In addition, the highly non-linear material properties coupled with the geometrical complexity, cause the structural analysis FRP bridges extremely more complex and challenging.

Integrated finite strip method as a very accurate and user friendly technique has the great potential to be extended for modelling the laminated FRP deck bridges. I this regard, so-called laminate spline strip is developed to model the anisotropic laminated FRP deck considering the coupling effects between flexural and membrane displacements of the FRP deck while the rapid convergence rate of the numerical results is still guaranteed. Integrating the laminate strips with the column strips, and transition section elements will provide the opportunity to model an FRP bridge in the environment of integrated finite strip method.

2. DEVELOPMENT OF LAMINATE SPLINE STRIP FOR DECK MODELLING

To model a composite FRP deck, a laminated FRP plate can be selected which is itself a collection of FRP lamina, arranged in a specified order. Adjacent lamina may be of the same or different materials, and their fiber orientations with respect to a reference axis may be arbitrary. In Figure 1, a rectangular flat multi-layer composite laminated FRP plate is shown. The classical lamination theory is used in the present study to derive the stiffness matrix of a composite laminated FRP plate in the environment of spline finite strip method. In the lamination theory, it is assumed that each lamina is in a state of plane stress while the interlaminar stresses are neglected. In addition, a perfect bonding between different laminas is assumed, which means that the laminated FRP plate behaves as a unity, homogenous, anisotropic plate.

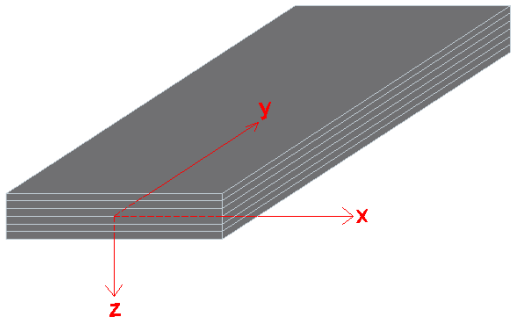

Figure 1: Multi-layer composite laminated plate

2.1 Displacement functions

The displacement of a laminate spline strip in the integrated finite strip method can be obtained by applying B3-spline functions in the longitudinal direction and the polynomials in the transverse direction of the strip. Figure 2 defines the coordinate system where its origin is assumed to be on the middle surface of the FRP laminated plate. As a result of assuming plane stress condition in each lamina, transverse shear strains are neglected. In addition, in-plane displacements are linear functions of the z coordinate and transverse normal strain is negligible. Considering these assumptions, the displacements of the FRP laminate at a general point can be expressed in terms of

[1] $\bar{u}(x,y,z) = u(x,y) + z\psi_x(x,y)$

[2] $\bar{v}(x,y,z) = v(x,y) + z\psi_y(x,y)$

[3] $\bar{w}(x,y,z) = w(x,y)$

where ψ_x and ψ_y are independent rotations while *u*, *v,* and *w* are displacements at the middle surface of the laminate along x, y, and z axes respectively.

2.2 Discretization by spline strips

In the environment of the spline finite strip method, each laminated FRP plate can be discretized into a number of strips. The laminate spline strip as shown in Figure 2 is developed for modeling the composite laminated FRP deck in which both in-plane and out-of-plane degrees of freedom are considered. The parameters in Figure 2 are defined in the following lines. In contrast with isotropic shell strip (Naderian et al. 2015), the coupling effects need to be investigated in analyzing the laminate spline strip.

In the case of flat laminates, one can consider four degrees of freedom on each knot of a nodal line of a spline strip, three translational and one rotation. The total potential energy of a flat laminate strip is obtained from algebraic summing the membrane (in-plane) and bending (out-of-plane) deformations. The displacement parameters vector of a laminate spline strip centered at y_m is given by

[4] $$\{\delta\}_m = \left[u_{im}, v_{im}, w_{im}, \theta_{im}, u_{jm}, v_{jm}, w_{jm}, \theta_{jm}\right]^T$$

In the formulation of the spline finite strip method it is better to have the locations of the supports and the concentrated load coinciding with the knots on the nodal lines, in order to obtain acceptable results. To reach this goal, unequally spaced B3-spline functions are used in the present study. Moreover, the introduction of unequally spaced interior knots allows one to describe the accurate response in the region of high stress gradients, or at the locations of abrupt geometric changes, by spacing knots more closely. In this case, the spline function centered at y_m can be expressed as

[5] $$F_m(y) = \begin{cases} 0 & y < y_{m-2} \\ A_m(y - y_{m-2})^3 & y_{m-2} \le y < y_{m-1} \\ A_m(y - y_{m-2})^3 + C_m(y - y_{m-1})^3 & y_{m-1} \le y < y_m \\ B_m(y_{m+2} - y)^3 + D_m(y_{m+1} - y)^3 & y_m \le y < y_{m+1} \\ B_m(y_{m+2} - y)^3 & y_{m+1} \le y < y_{m+2} \\ 0 & y_{m+2} \le y \end{cases}$$

in which

[6] $$\begin{aligned} A_m &= \left[(y_{m+1} - y_{m-2})(y_m - y_{m-2})(y_{m-1} - y_{m-2})\right]^{-1} \\ B_m &= \left[(y_{m+2} - y_{m-1})(y_{m+2} - y_m)(y_{m+2} - y_{m+1})\right]^{-1} \\ C_m &= -(y_{m+2} - y_{m-2})\left[(y_{m+2} - y_{m-1})(y_{m+1} - y_{m-1})(y_m - y_{m-1})(y_{m-1} - y_{m-2})\right]^{-1} \\ D_m &= -(y_{m+2} - y_{m-2})\left[(y_{m+1} - y_{m-2})(y_{m+1} - y_{m-1})(y_{m+1} - y_m)(y_{m+2} - y_{m+1})\right]^{-1} \end{aligned}$$

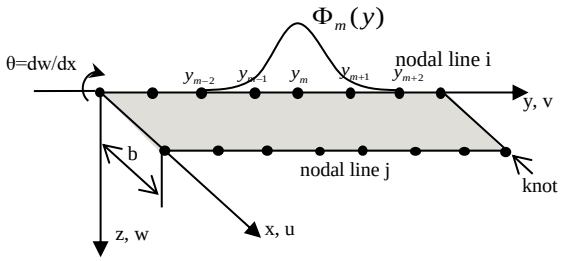

Figure 2: Laminate spline finite strip

The membrane displacement functions *u* and *v*, and the flexural displacement function *w* at the middle surface of the laminate can be expressed as the product of transverse polynomials and longitudinal B3-splines as following

[7] $u = \sum_{m=-1}^{r+1} (N_1 \Phi_{1m}(y) u_{im} + N_2 \Phi_{5m}(y) u_{jm})$

[8] $v = \sum_{m=-1}^{r+1} (N_1 \Phi_{2m}(y) v_{im} + N_2 \Phi_{6m}(y) v_{jm})$

[9] $w = \sum_{m=-1}^{r+1} (N_3 \Phi_{3m}(y) w_{im} + N_4 \Phi_{4m}(y) q_{im} + N_5 \Phi_{7m}(y) w_{jm} + N_6 \Phi_{8m}(y) q_{jm})$

where r is the total number of longitudinal sections on a nodal line and

[10] $N_1 = 1 - X,\ N_2 = X,\ N_3 = 1 - 3X^2 + 2X^3,\ N_4 = x(1 - 2X + X^2),\ N_5 = (3X^2 - 2X^3),\ N_6 = x(X^2 - X)$

in which $X = x/b$, and Φ_{1m} to Φ_{8m} are the longitudinal shape functions; Φ_{1m}, Φ_{2m}, Φ_{5m} and Φ_{6m} are related to displacements *u* and *v* of nodal lines *i* and *j* respectively while Φ_{3m}, Φ_{4m}, Φ_{7m} and Φ_{8m} are related to displacement *w*. The longitudinal shape functions consist of (m+3) local B3-splines. Each longitudinal shape function has the following form

[11] $[\Phi] = \left[\bar{\Phi}_{-1} \quad \bar{\Phi}_0 \quad \bar{\Phi}_1 \quad \Phi_2 \quad \ldots \quad \Phi_{m-2} \quad \bar{\Phi}_{m-1} \quad \bar{\Phi}_m \quad \bar{\Phi}_{m+1} \right]$

where $\bar{\Phi}_i$ is an amended local boundary spline with regard to the end boundary conditions of the strip.

2.3 Constitutive equations

The following constitutive equations relates the stresses to the strains in an arbitrary lay-up laminate spline strip

[12] $$\begin{Bmatrix} N_x \\ N_y \\ N_{xy} \\ M_x \\ M_y \\ M_{xy} \end{Bmatrix} = \begin{bmatrix} A_{11} & & & & & \\ A_{12} & A_{22} & & Sym & & \\ A_{16} & A_{26} & A_{66} & & & \\ B_{11} & B_{12} & B_{16} & D_{11} & & \\ B_{12} & B_{22} & B_{26} & D_{12} & D_{22} & \\ B_{16} & B_{26} & B_{66} & D_{16} & D_{26} & D_{66} \end{bmatrix} \begin{Bmatrix} \varepsilon_x \\ \varepsilon_y \\ \gamma_{xy} \\ \kappa_x \\ \kappa_y \\ \kappa_{xy} \end{Bmatrix}$$

in which $\varepsilon_x, \varepsilon_y, \gamma_{xy}$ and $\kappa_x, \kappa_y, \kappa_{xy}$ are mid-surface strains and curvatures respectively, while N_x, N_y, N_{xy}

are membrane and shear forces per unit length and M_x, M_y, M_{xy} are the bending and twisting moments per unit length in the middle surface of the laminate spline strip, while . A_{ij}, B_{ij}, and D_{ij} are the components relating to laminate extensional stiffness, laminate-coupling stiffness, and laminate-bending stiffness matrices respectively and are obtained by the following integrations (Gibson 2012)

[13] $A_{ij} = \int_{-t/2}^{t/2} (\bar{Q}_{ij)}{}_k \, dz = \sum_{k=1}^{N} (\bar{Q}_{ij)}{}_k (z_k - z_{k-1})$

[14] $B_{ij} = \int_{-t/2}^{t/2} (\bar{Q}_{ij)}{}_k z \, dz = \frac{1}{2} \sum_{k=1}^{N} (\bar{Q}_{ij)}{}_k (z_k^2 - z_{k-1}^2)$

[15] $D_{ij} = \int_{-t/2}^{t/2} (\bar{Q}_{ij)}{}_k z^2 \, dz = \frac{1}{3} \sum_{k=1}^{N} (\bar{Q}_{ij)}{}_k (z_k^3 - z_{k-1}^3)$

where the subscripts i, j=1,2, or 6; N is the number of laminas; t is the laminate thickness; z_k and z_{k-1} are distances from middle-surface to inner and outer surfaces of the k_{th} lamina respectively as illustrated in Figure 3.

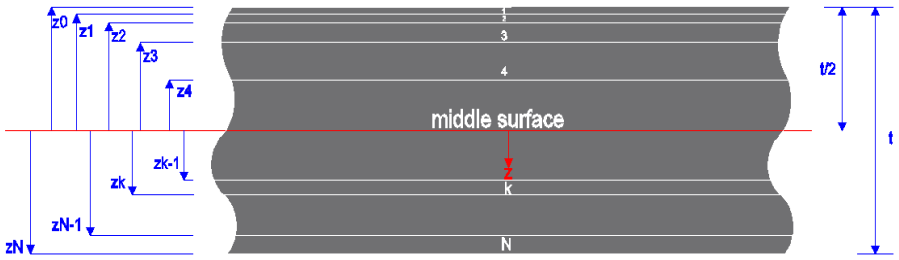

Figure 3: Laminated plate cross-sectional geometry and ply numbering system

The coupling stiffness matrix couples the in-plane forces with the curvatures and the moments with the mid-plane strains. In fact, the coupling at laminate is not related to material anisotropy but is due to geometric and/or material property asymmetry with respect to the middle surface. In Eqs. 13 to 15, $(\bar{Q}_{ij)}{}_k$ are the components of the transformed k^{th} lamina stiffness matrix as below

$$\bar{Q}_{11} = Q_{11}c^4 + Q_{22}s^4 + 2(Q_{12} + 2Q_{66})s^2c^2$$
$$\bar{Q}_{12} = (Q_{11} + Q_{22} - 4Q_{66})s^2c^2 + Q_{12}(c^4 + s^4)$$
$$\bar{Q}_{22} = Q_{11}s^4 + Q_{22}c^4 + 2(Q_{12} + 2Q_{66})s^2c^2$$
$$\bar{Q}_{16} = (Q_{11} - Q_{12} - 2Q_{66})c^3s - (Q_{22} - Q_{12} - 2Q_{66})cs^3$$
$$\bar{Q}_{26} = (Q_{11} - Q_{12} - 2Q_{66})cs^3 - (Q_{22} - Q_{12} - 2Q_{66})c^3s$$
[16] $$\bar{Q}_{66} = (Q_{11} + Q_{22} - 2Q_{12} - 2Q_{66})s^2c^2 + Q_{66}(s^4 + c^4)$$

where c=cos θ, s=sin θ, and θ is the lamina orientation angle while Q_{ij} are the components of the lamina stiffness matrix which are related to the engineering constants as follows

[17] $Q_{11} = \frac{E_1}{1-\nu_{12}\nu_{21}}$, $Q_{12} = \frac{\nu_{12}E_2}{1-\nu_{12}\nu_{21}}$, $Q_{22} = \frac{E_2}{1-\nu_{12}\nu_{21}}$, $Q_{66} = G_{12}$

in which E_1 and E_2 are modulus of elasticity of the lamina in longitudinal and transverse directions respectively, while ν_{12} and ν_{21} are the corresponding Poison's ratios respectively and G_{12} is the shear modulus of the lamina.

3. INTEGRAED FINITE STRIP SOLUTION

In IFSM, the so-called Column Strip is used for modeling the cantilever-behaved piers. The Column Strip is exactly similar to the flat shell spline finite strip. However, Column Strip is a vertical strip fixed at one end, for providing the support boundary conditions, and free at the other end, as shown in Figure 4.

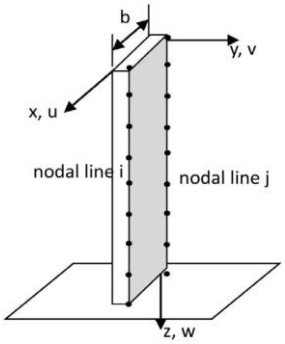

Figure 4: Three dimensional column strip in local coordinate system (Naderian et al. 2015)

The concept “element” in the longitudinal direction is not defined neither in the ordinary finite strip method, nor in spline the finite strip method. In order to solve this problem, a special transition section has been developed within the IFSM, which is applied to connect the FRP deck and piers together. The transition section is developed by using unequal spaced B3-spline functions. The bearings can be modeled as special boundary conditions for the transition section. A typical transition section connecting the deck with the pier is shown in Figure 5. Not losing generalization, it is assumed that the width of the normal and the transition sections are *H* and *h* respectively. One can call the vertical line as a nodal line on the pier strip and the horizontal line as a nodal line on the laminated FRP deck strip. The vertical and horizontal lines overlap at knots 3 and 8 of the deck and the pier strips, respectively. To model a fixed bearing, which allows rotations but restricts translations, for example, the knot 3 and knot 8 should have the same displacement value to achieve compatibility. In order to have identical displacement at knots 3 and 8, it is obvious that the ratio of h/H should be infinitely small. Using the developed transition section in the spline finite strip procedure, the compatibility for the displacements of different components of the structure is satisfied.

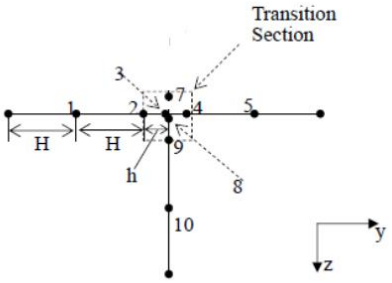

Figure 5: Transition section

The material properties of each layer of the FRP laminated deck including engineering constants as well as the FRP ply angle are modelled by laminate spline strips. A three dimensional column strip model the piers of the FRP bridge. The principle of the minimum potential energy following the standard finite element procedure can be used to derive the stiffness and mass properties of the laminate strips and column strips. In the IFSM, the strip properties are converted to knots along the nodal lines during the simulating process. However, the number of required knots is significantly reduced comparing to FEM due to the semi-analytical nature of the IFSM. The stiffness and mass matrices as well as the force vectors of all the strips are assembled using conventional assembling procedure. Then, the entire 3D model of the FRP bridge is built using IFSM. When assembling the whole FRP Bridge, the connectivity

between the FRP deck and pier is provided by transition section elements which have already been defined in the formulation of each individual strip.

4. INTEGRATED FINITE STRIP MODELING OF MULTI-SPAN FRP SLAB-GIRDER BRIDGE

To verify the accuracy and efficiency of the proposed integrated finite strip solution for both bending and free vibration analysis, a short span hybrid FRP slab-girder bridge, as shown in Figure 6(a), is presented. The layout of the FRP laminated deck consists of 10 layers of 2 cm thickness CFRP lamina, with the orientation configuration of [0, 90, 0, 90, 0, 0, 90, 0, 90, 0] degrees. The FRP is made by CFRP (IM6G/3501-6) with the following properties: mass density $\rho = 1600\ (kg/m^3)$, $E_1 = 147\ GPa$, $E_2 = 10\ GPa$, $G_{12} = 7\ GPa$, and ν_{12}=0.25. The pier is made from concrete with the modulus of elasticity $E = 3.0\times10^4$ MPa , the Poisson's ratio of 0.2, and the material density is 2,500 kg/m^3. Both IFSM and FEM are adopted to model the bending and free vibration behavior of the structure, and the results are compared.

A full bridge model is constructed using the laminate strip for the FRP deck, 3D column strip (CS) for the pier and the transition section elements for the bearings. The deck is divided into four equal strips, and the pier is divided into two CSs. Each deck strip is composed of 32 sections as well as two additional transition sections. Each pier strip is composed of 4 sections, as well as one transition section. For FEM, the mass and stiffness of the bridges is constructed with five degrees-of-freedom shell elements throughout the structure. The deck is meshed with 32 by 4 elements, and the pier is meshed with 4 by 2 elements.

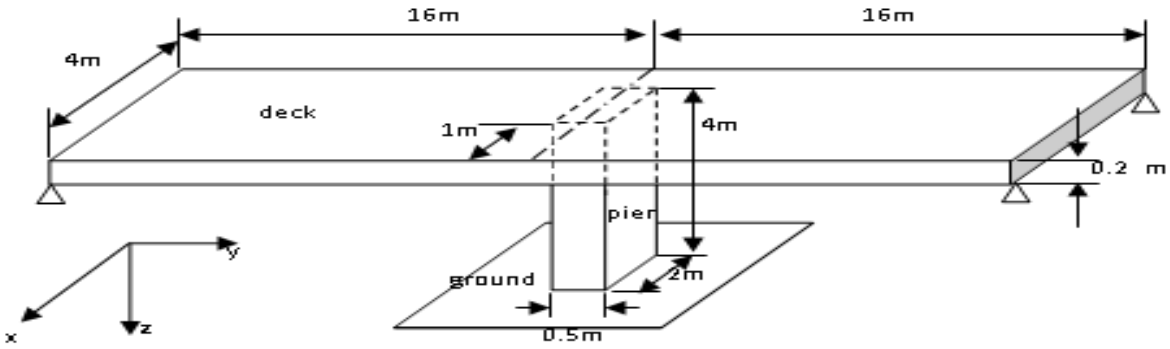

(a)

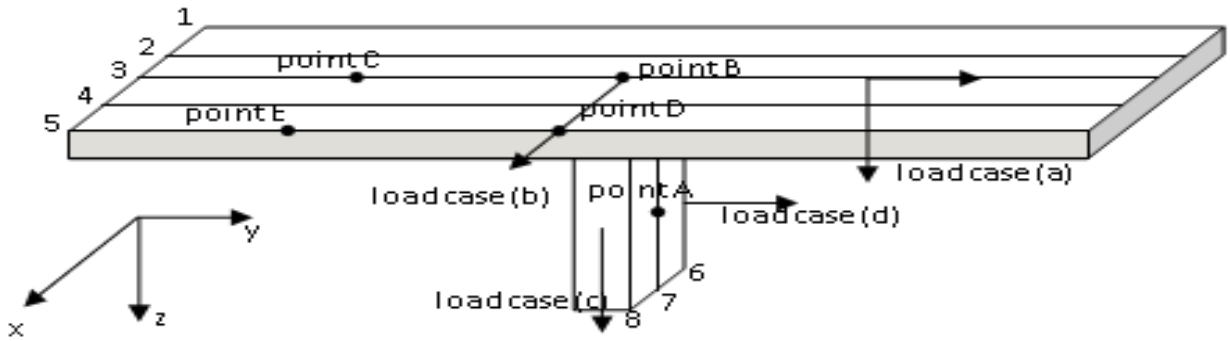

(b)

Figure 6: An FRP slab girder bridge: (a) structural Layout; (b) loading patterns

4.1 Bending performance

For the bending analysis, the ability of the transition element to transfer loading between the laminate deck strip and the column strip is assessed. Three load cases, with constant 1,000 KN point forces acting on different components and in different directions, are assigned to the model as shown in Figure 6(b). The vertical and horizontal drifts along different nodal lines, determined from both numerical methods, are summarized in Tables 1 to 3. It was noticed that the displacement calculated from the integrated approach agrees well with the FEM results for all loading conditions, which indicates that the proposed approach can successfully model a FRP deck bridge structure in the FS environment, taking the pier-bearing-deck interaction as well as coupling effects of composite deck into consideration.

Table 1: Displacements under load case (a)

Case a		Deck-nodal line 3					Pier-nodal line 7		
	Y (m)	0 (left)	8	16	24	32 (right)	z (m)	0 (top)	2
v (mm)	IFSM	0.072	0.105	0.156	0.275	0.145	IFSM	0.149	0.048
	FEM	0.073	0.110	0.166	0.302	0.149	FEM	0.166	0.052
w (mm)	IFSM	-1.696	-150.121	0.060	470.458	6.705	IFSM	0.071	0.046
	FEM	-1.580	-174.372	0.068	450.783	6.856	FEM	0.068	0.046

Table 2: Displacements under load case (b)

Case b		Deck-nodal line 3					Pier-nodal line 7		
	Y (m)	0	8	16	24	32	z (m)	0	2
u (mm)	IFSM	0.001	0.832	1.813	0.983	0.004	IFSM	1.486	0.598
	FEM	0.003	0.832	1.605	0.832	0.003	FEM	1.605	0.527

Table 3: Displacements under load case (d)

Case d		Deck-nodal line 2					Pier-nodal line 6		
	Y (m)	0	8	16	24	32	z (m)	0	2
v (mm)	IFSM	0.034	0.055	0.089	0.048	0.030	IFSM	0.139	1.836
	FEM	0.031	0.053	0.115	0.062	0.010	FEM	0.115	1.733

4.2 Free vibration analysis

Table 4 compares the first 7 natural bending frequencies of the models. The very small deviation of the modal frequencies between the two methods demonstrates that the integrated approach is capable of capturing the free vibration characteristics of a bridge, whereas the minor deviation is likely to be caused by the slight differences in mass distribution within different elements. The deformed shape of the FRP slab girder bridge for the first seven natural modes are illustareted in Figure 7.

Table 4: Natural Frequency of the FRP slab Bridge

Mode Number	Frequency (Hz)		Mode Shape
	Integrated FSM	FEM	
1	2.08	2.00	Heave (deck) antisymmetrical
2	3.38	3.11	Heave (deck) symmetrical
3	8.08	7.90	Heave (deck) antisymmetrical
4	10.78	9.90	Heave (deck) symmetrical
5	17.59	17.33	Torsional (deck) antisymmetrical
6	19.60	19.96	Torsional (deck) symmetrical
7	29.47	29.38	Heave (deck) antisymmetrical

(a) First mode (2.08 Hz) (b) Second mode (3.38 Hz)

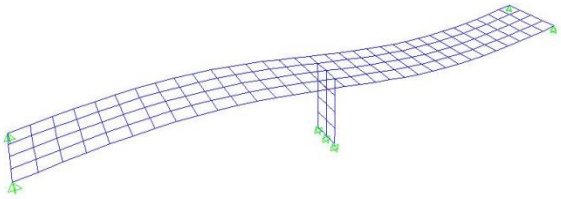

(c) Third mode (8.08 Hz)

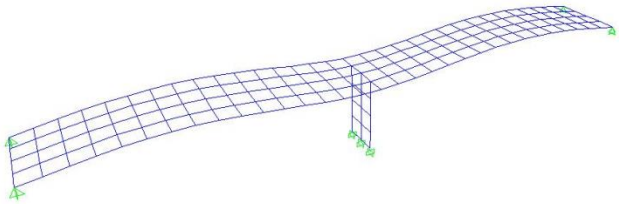

(d) Fourth mode (10.78 Hz)

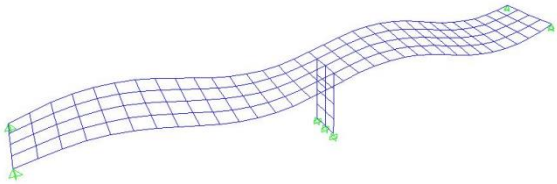

(e) Fifth mode (17.59 Hz)

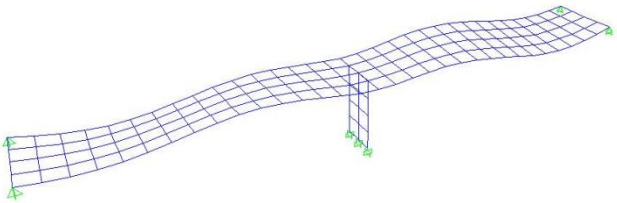

(f) Sixth mode (19.60 Hz)

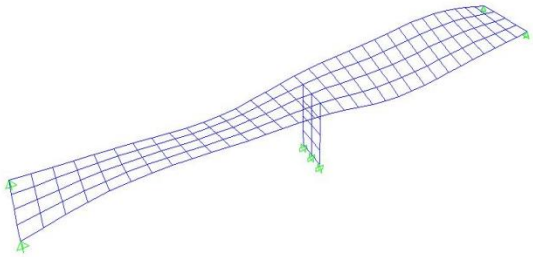

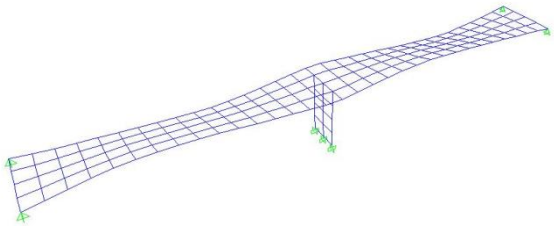

(g) Seventh mode (29.47 Hz)

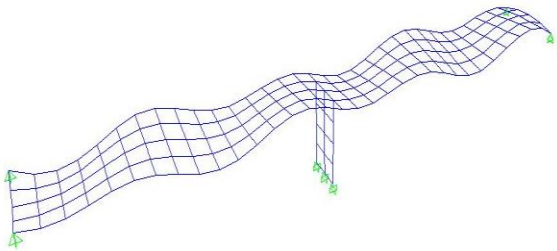

Figure 7: Mode shapes of the FRP slab-girder bridge

As further studies, and in order to compare the free vibration performance of an FRP deck bridge with a concrete deck bridge, the natural frequencies of both systems are compared in Table 5. The material properties of the deck are the same as for the pier, while the thickness of the concrete deck is 25 cm. The integrated finite strip results show that the natural frequencies of the FRP bridge are higher than those of the concrete bridge because the total weight of the FRP deck is reduced due to the use of the FRP material instead of concrete. In other words, the stiffness to mass ratio has increased in FRP bridge comparted to the concrete bridge. Comparing the mode shapes of the two bridges, it can be concluded that the torsional mode is more likely to occur in the FRP bridge model. Therefore, special attention

needs to be paid to investigating the torsional instability of FRP bridges. The latter proves that the dynamic behaviour of the FRP bridge is totally different from the concrete bridge one.

Table 5: Comparison of natural frequencies of FRP and concrete bridges

Mode	Frequency (Hz)		Mode Shape	
	FRP bridge	Concrete bridge	FRP bridge	Concrete bridge
1	2.08	1.53	Heave (deck) antisymmetrical	Heave (deck) antisymmetrical
2	3.38	2.40	Heave (deck) symmetrical	Heave (deck) symmetrical
3	8.08	6.11	Heave (deck) antisymmetrical	Heave (deck) antisymmetrical
4	10.78	7.73	Heave (deck) symmetrical	Heave (deck) symmetrical
5	17.59	13.57	Torsional (deck) antisymmetrical	Heave (deck) antisymmetrical
6	19.60	15.77	Torsional (deck) symmetrical	Heave (deck) symmetrical
7	29.47	22.45	Heave (deck) antisymmetrical	Heave (deck) antisymmetrical

5. CONCLUDING REMARKS

An efficient integrated finite strip framework is deployed for continuous multi-span FRP bridges in the environment of spline finite strip method. The so-called laminate strip can model the FRP deck considering the coupling effects between the in-plane and out-of-plane degrees of freedom as well as the anisotropic material properties of the laminated FRP deck. The other components of the bridge can also be modelled by spline based finite strips. 3D column strips model the piers, while the transition section elements combine the strips of different orientations. The application of the laminate strip along with the integrated finite strip method resulted in a very precise and efficient numerical technique for modelling the FRP based bridge structures. The application of the proposed finite scheme was extended for bending, and free vibration. The finite strip results of bending analysis and natural frequencies and mode shapes of an FRP slab-girder bridge were compared with those obtained by finite element method and a very good agreement was witnessed. Among the advantages of the proposed solution are the high efficiency and accuracy as well as minimal computational time and the simplicity of input data.

Acknowledgements

The authors wish to gratefully acknowledge the financial support of Canada NSERC Industrial Postgraduate Scholarship.

References

Cheung, M. S., Li, W. and Chidiac, S. E. 1996. **Finite strip analysis of bridges**. 1st Ed., E & FN Spon, London, New York, USA.

Naderian, H., Cheung, M.S., Shen, Z., Dragomirescu, E., 2015. Integrated Finite Strip Analysis of long-span cable-stayed bridges, **Computers and Structures** 158 (2015) 82–97

Reddy, J. 2004. *Mechanics of Laminated Composite Plates and Shells: Theory and Analysis*, CRC Press, New York, USA.

Gibson, R. F. 2012. **Principles of Composite Material Mechanics**, 4th Ed. CRC Press, New York, USA.